



Sensibility study of flooding and drying issues to the operating conditions in PEM fuel cells

F. Brèque¹, J. Ramousse², Y. Dubé¹, K. Agbossou¹, P. Adzakpa¹

¹ Hydrogen Research Institute, Université du Québec à Trois-Rivières, 3351 boulevard des Forges, C.P. 500, Trois-Rivières (Québec), G9A 5H7, Canada.

² LOCIE - Université de Savoie, Campus scientifique - Savoie Technolac, 73376 Le Bourget du Lac – CEDEX, France.

Abstract

Due to water management issues, operating conditions need to be carefully chosen in order to properly operate fuel cells. Because of the gas consumption along the feeding channels and water production at the cathode, internal cell humidification is highly inhomogeneous. Consequently, operating fuel cells are very often close to critical operating conditions, such as flooding and drying, at least locally. Based on this observation, the critical current, corresponding to internal cell humidification balance (accurate membrane hydration, without excess of water at the electrodes), is deduced from a pseudo-2D model of mass transfer in the cell. Using the model, a parametric sensibility study of the operating conditions is presented to analyze the cell internal humidification. Dead-end and flow-through modes of hydrogen supply are also compared.

It is shown that the operating temperature is a key parameter to manage the cell humidification. Moreover, although the oxygen stoichiometric ratio has an effect on cell humidification, this influence is limited and cannot be used alone to adjust the cell humidification. Furthermore, it is shown that in some cases, humidifying the anode inlet gas is of little interest to the internal humidification adjustment. Finally, those results allow to understand the role that each operating parameter can play on the cell internal humidification. Consequently, this study is of a great interest to water management improvement in polymer electrolyte membrane fuel cells.

Copyright © 2010 International Energy and Environment Foundation - All rights reserved.

Keywords: Hydrogen supply modes, Modeling, Parametric sensibility study, Polymer electrolyte membrane fuel cell, Water management.

1. Introduction

Among possible alternatives to global warming and energy resource depletion problems, polymer electrolyte membrane fuel cells (PEMFC) appear as promising energy conversion devices using hydrogen as energy vector. They are environmentally friendly and more efficient than standard combustion engines [1]. In order to achieve high performances, water management in PEMFCs is one of the main critical issues to address: lack of water in the membrane can lead to an important increase of membrane resistance and thus to a decrease of the cell potential, while an excess of liquid water in the electrodes can reduce gas transport to the catalyst layers and, again, decrease the cell voltage. The lack of

humidification (drying) and excess of humidification (flooding) are thus harmful to the performances of the PEMFC [2]. Accurate water content is therefore required in the cell.

In this context, numerical models combined with experimentation can help to understand the mechanisms involved in the cell operation, and thus can lead to water management improvement. The bases of the PEMFC modeling have been set in the early 90's: 1D isothermal and steady state models of PEMFCs were developed [3, 4]. Later, the channel dimension and primary temperature effects were added to the models [5-7] in order to describe the non-homogeneous distribution of the species and temperature in the cell. The main mechanisms driving the cell performances were thus pointed out.

Using models, the main influences of the operating parameters on gaseous species and liquid water distributions were studied [8, 9]. These authors highlighted the decrease of performances caused by liquid water accumulation along the channels. In parallel to those numerical results, experimental studies were also conducted. The effect of the cell internal humidification on the cell voltage was experimentally pointed out [11, 15] and the local water accumulation in a cell was observed using neutron imaging procedure [10, 12]. Finally, all these numerical and experimental studies confirm that liquid water has major effects on fuel cell performances. According to this observation, it is needed to predict the influences of the operating conditions on the internal cell humidification as well as on the cell performances.

In this way, the threshold current density corresponding to the onset of two-phase operating regimes have already been derived thanks to simple analytical expressions [12, 14] or more detailed models [16, 17]. Even though influences of some operating parameters on the internal cell humidification have been analyzed, no comprehensive studies on the effect of all the operating parameters on the cell performances have been presented. Moreover, no information in terms of appropriate operating parameters (accurate membrane hydration without water excess in the electrodes) are given, though such information is the most important aspect when studying water management in fuel cells. Consequently, information given by those models is not sufficient to develop a water management strategy. Moreover, to our knowledge, no comparison between the different modes of hydrogen supply (dead-end or flow-through) has been conducted. Few experimental studies were also conducted on the influence of operating parameters [18] but more numerical work is needed in order to improve water management strategies.

For that purpose, a complete sensibility analysis of the internal humidification is presented in this paper. This study is based on a dynamic pseudo-2D model of mass transfer in a polymer electrolyte membrane fuel cell. This model describes multi-component gas transport in the electrodes and water transport in the membrane. As a result, the effects of operating conditions on liquid water appearance in the cell and on the related cell performances are discussed and analyzed in detail. These operating conditions include relative humidities, temperatures, pressures and stoichiometric ratios at both electrodes, as well as the modes of hydrogen supply (flow-through or dead-end). Hence, for any given operating condition, the critical operating current leading to a well-hydrated membrane without water excess in the electrodes is computed.

Because the model applies for a specific fuel cell, the results are based on given fuel cell features like geometry. Therefore, the critical operating current presented here refers of course to the modeled fuel cell and is not necessarily the same for other fuel cells. However, the method and the tendencies of the results presented are more general. Based on this model, the role that each operating parameters can play in order to manage the internal cell humidification is pointed out. According to these results, a control strategy will next be developed to operate any modeled cell at the best humidification conditions.

2. Numerical modeling

2.1 Mathematical problem statement

The modeled single fuel cell is represented schematically in Figure 1. The input gases, hydrogen at the anode and oxygen at the cathode, flow in channels in the z -direction. Both flows reach the catalyst layers (CL) by transport through the two GDLs (x -direction). There, reactants are consumed and water is produced at the cathode side. The water flowing in the membrane is absorbed on one side and desorbed on the other.

The following transport phenomena are taken into account. First, the motion of the gas molecules can be either by bulk transport, by convection, and/or by diffusion. Second, the gases fed in are not pure, but contain nitrogen (in the air), water and trace concentrations of other gases (CO, nitrogen compounds etc.) whose effects have to be taken into account. Third, the motion of the water molecules inside the membrane is also affected by electro-osmotic drag, which corresponds to the water transport relating to

the proton transport from the anode to the cathode, and which acts in addition to the usual convection and diffusion. And fourth, from a practical point of view, the hydrogen supply can be either flow-through or dead-end (the air supply is always flow-through).

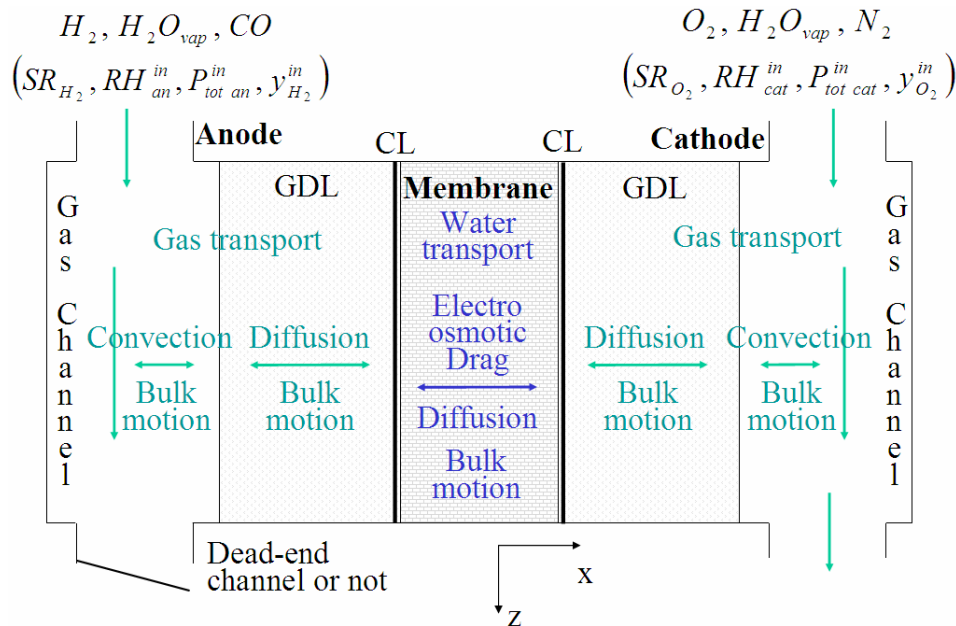


Figure 1. Schematic of mass transfer phenomena in PEM fuel cells

The main assumptions considered in the model are as follows [19]:

- The model is a pseudo 2D model. The model computes species flow in the channel direction, but current density in the z -direction is assumed constant. Water fluxes at the membrane interfaces are also assumed to be constant in the z -direction.
- The cell temperature remains uniform in the cell [20].
- The total pressures remain uniform in both GDLs [20].
- Species are considered in gas phase only (no liquid water) in the gas channels and in the GDLs. 2-phase water transport in the electrodes will be introduced in future work. The gas phase is treated as an ideal mixture.
- The cathode CL is integrated in the membrane to model water production while the anode CL is assumed to be infinitely thin as explained in [21].
- Gas crossover in the membrane is neglected.

2.2 Membrane water transport (x -direction)

Water transport in the membrane is modeled with the governing equations proposed by Springer et al. [4] and used by Fournier et al. [19]. Water concentration in the membrane and in the cathode CL follows the continuity equation (1).

$$\frac{\partial C_w}{\partial t} + \frac{\partial N_w}{\partial x} = \begin{cases} 0 & \text{in the membrane} \\ R_w & \text{in the cathode catalyst layer} \end{cases} \quad (1)$$

where C_w is the water concentration (mol.m^{-3}), t is time (s), N_w is the water molar flux ($\text{mol.m}^{-2}.\text{s}^{-1}$) and x the abscissa (m) and R_w the molar water production rate ($\text{mol.m}^{-3}.\text{s}^{-1}$).

The water concentration C_w is related to the water content λ ($\text{mol}_{H_2O} / \text{mol}_{SO_3}$) by equation (2) (λ is the ratio between the water moles and the sulfate sites moles in the membrane):

$$\lambda = \frac{EW}{\rho_m} C_w \quad (2)$$

where EW and ρ_m are respectively the equivalent weight of the membrane ($kg \cdot mol_{SO_3}^{-1}$) and the density of the dry membrane ($kg \cdot m^{-3}$).

The molar water production rate (assumed uniform in the CL thickness) in the catalyst layer R_w is given according to Faraday's law:

$$R_w = \frac{i}{2L^{int}F} \quad (3)$$

where i is the current density ($A \cdot m^{-2}$), L^{int} is the cathode catalyst layer thickness (m) and F is the Faraday's constant ($F=96485 C \cdot mol^{-1}$)

Water transport across the membrane is driven by three phenomena: diffusion [4], electro-osmotic drag [4] and bulk motion [22]. Therefore the water flux across the membrane N_w is given by equation (4):

$$N_w = -D_w \frac{\partial C_w}{\partial x} + \eta_d \frac{i}{F} + C_w v \quad (4)$$

where D_w is the water diffusivity in the membrane ($m^2 \cdot s^{-1}$), η_d is the electro-osmotic drag coefficient (-) and v is the total velocity ($m \cdot s^{-1}$).

In equation (4), the first term describes the diffusion in which D_w the water diffusivity in the membrane, is based on [4]:

$$D_w = D_\lambda \exp \left[2416 \left(\frac{1}{303} - \frac{1}{T_{op}} \right) \right] \quad (5)$$

where T_{op} is the cell operating temperature (K) and D_λ ($m^2 \cdot s^{-1}$) depends on λ as follow:

$$D_\lambda = \begin{cases} 1.03125 \times 10^{-11} \lambda & \text{if } \lambda \leq 3 \\ 1.744 \times 10^{-11} \lambda - 2.14 \times 10^{-11} & \text{if } 3 < \lambda \leq 6 \\ 5.766 \times 10^{-12} \lambda + 4.8656 \times 10^{-11} & \text{if } \lambda > 6 \end{cases} \quad (6)$$

The second term in equation (4) is the electro-osmotic drag and is proportional to the current density with a water content dependant coefficient [4]:

$$\eta_d = \frac{2.5}{22} \lambda \quad (7)$$

The last term in equation (4) refers to the bulk motion, usually called convection. The velocity v is computed via Darcy's law with a linearity assumption on the total pressure in the membrane:

$$v = -\frac{K}{\mu} \frac{\partial P}{\partial x} = \frac{K}{\mu} \left(\frac{P_{an} - P_{cat}}{L_m} \right) \quad (8)$$

where K is the membrane permeability (m^2), μ is the water viscosity ($kg \cdot m^{-1} \cdot s^{-1}$), P is the pressure (Pa) denoted P_{an} at the anode and P_{cat} at the cathode, and L_m is the membrane thickness (m).

The boundary conditions for (1) are the water content at both membrane/GDL interfaces. These water contents are computed from the water pressure at the membrane/GDL interface via the sorption isotherm [4]. The sorption isotherm represents the balance between the water activity A (-) in the gas and the membrane water content λ at the membrane/GDL interface:

$$\lambda = 0.043 + 17.81 A - 39.85 A^2 + 36.0 A^3 \quad \text{for } 0 < A \leq 1 \quad (9)$$

where

$$A = \frac{P_w^{\text{int}}}{P_{\text{sat}}(T_{\text{op}})} \quad (10)$$

with P_w^{int} is the water pressure at the membrane/cathode interface (Pa) and P_{sat} the vapor saturation pressure (Pa) is given by (11) in [4]:

$$\log_{10} \frac{P_{\text{sat}}}{P_0} = 1.4454 \times 10^{-7} (T_{\text{op}} - 273.15)^3 - 9.1837 \times 10^{-5} (T_{\text{op}} - 273.15)^2 + 0.02953 (T_{\text{op}} - 273.15) - 2.1794 \quad (11)$$

where P_0 is the reference pressure (1 atm).

2.3 GDL transport model (x-direction)

Gaseous species involved are respectively H_2 , H_2O_{vap} and CO at the anode and O_2 , H_2O_{vap} and N_2 at the cathode. Their distribution in the GDLs are computed with the species conservation [13] in a one-phase flow:

$$\frac{\partial}{\partial t} \left(\frac{P_{\text{tot}}}{RT_{\text{op}}} \varepsilon y_i \right) + \frac{\partial}{\partial x} (y_i N_{\text{tot}}) = - \frac{\partial}{\partial x} \left(- \frac{P_{\text{tot}}}{RT_{\text{op}}} D_{\text{im}}^{\text{eff}} \frac{\partial}{\partial x} (y_i) \right) \quad (12)$$

where R is the universal gas constant ($R=8.314 \text{ J}\cdot\text{mol}^{-1}\cdot\text{K}^{-1}$), ε is the GDL porosity (-) and y_i the molar fraction of species i (-) defined by (13):

$$y_i = \frac{P_i}{P_{\text{tot}}} \quad (13)$$

The term $y_i N_{\text{tot}}$, where $N_{\text{tot}} = \sum N_i$, refers to the bulk motion. The right part of equation (12) corresponds to the diffusion. The effective gas diffusivity of species i in the mixture m $D_{\text{im}}^{\text{eff}}$ ($\text{m}^2\cdot\text{s}^{-1}$) is given by:

$$D_{\text{im}}^{\text{eff}} = \frac{P_j D_{ij}^{\text{eff}} + P_k D_{ik}^{\text{eff}}}{P_j + P_k} \quad (14)$$

where j and k are the two other species of the gas mixture. Effective diffusivity refers to the diffusivity in a porous medium. In the case of a random fibrous porous medium, Nam and Kaviany [23] derived the effective diffusivity as follow.

$$D_{ij}^{\text{eff}} = D_{ij} \varepsilon \left(\frac{\varepsilon - \varepsilon_p}{1 - \varepsilon_p} \right)^\alpha \quad (15)$$

where $\varepsilon_p = 0.11$ and $\alpha = 0.785$.

The binary gas diffusivity of the species i within j D_{ij} is computed similarly as proposed by Bird et al. [24].

Fluxes at the membrane/GDL interfaces are boundary conditions for (12). Except for water, these fluxes are computed according to Faraday's law:

$$N_{H_2} = \frac{i}{2F}, N_{O_2} = -\frac{i}{4F}, N_{N_2} = N_{CO} = 0 \quad (16)$$

N_{H_2O} is given as an output of the membrane sub-module.

The other boundary conditions for equation (12) are the molar fractions at the GDL/gas channel interface $y_i^{\text{GDL}/\text{ch}}$. They are computed according to equation (17):

$$N_i = -h_m \frac{P_{\text{tot}}}{RT_{\text{op}}} (y_i^{\text{ch}} - y_i^{\text{GDL}/\text{ch}}) + y_i N_{\text{tot}} \quad (17)$$

where h_m is the mass transfer convection coefficient ($\text{m}\cdot\text{s}^{-1}$) which is fixed using the Sherwood number [25].

This equation expresses, in steady state, the mass transport between the bulk molar fraction in the channel y_i^{ch} and the molar fraction at the GDL/channel interfaces. The last term in equation (17) corresponds to the bulk motion of the mixture. The molar fraction y_i is either $y_i^{GDL/ch}$ or y_i^{ch} depending on the direction of the bulk motion.

2.4 Channel transport model (z-direction)

Whereas air is supplied in flow-through mode only, hydrogen can be supplied in flow-through mode or in dead-end mode. To describe gas transport in each mode, two models are developed.

2.4.1 Flow-through mode

For each species, the molar balance for a slice ∂z in the channel is derived as:

$$\frac{\partial Q_i}{\partial z} = N_i \frac{A_m}{L_{ch}} \quad (18)$$

where the molar flux in the x-direction N_i is assumed to be uniform along the z-direction. The molar flows in the z-direction Q_i ($\text{mol}\cdot\text{s}^{-1}$) are as follow:

$$Q_i = \frac{P_i^{ch}}{R T_{op}} v_{tot} A_{ch} \quad (19)$$

In (19), the velocity of the total gas mixture in the channel v_{tot} ($\text{m}\cdot\text{s}^{-1}$) is computed in each slice using the relationship (20).

$$Q_{tot} = \frac{P_{tot}}{R T_{op}} v_{tot} A_{ch} \quad (20)$$

where A_{ch} is the channel area (m^2) and P_{tot} the total pressure in the slice ∂z , based on the total pressure drop in the channel. The total pressure drop is given by equation (21) [26]:

$$\Delta P_{tot} = k_1 Q_{tot} - k_2 \quad (21)$$

where Q_{tot} is the total molar flow ($\text{mol}\cdot\text{s}^{-1}$); the constants k_1 and k_2 are determined experimentally: $k_1 = 4.09 \cdot 10^{-3} \text{ atm} \cdot \text{s} \cdot \text{mol}^{-1}$ and $k_2 = 6.75 \cdot 10^{-4} \text{ atm}$. The decreasing total pressure along the channel direction is then assumed to be linear.

Using (18) to (21), the profiles of the partial pressures in the gas channel P_i^{ch} are computed along the z-direction.

2.4.2 Dead-end mode

In addition to the previous approach corresponding to flow-through mode, hydrogen can be supplied in dead-end mode. In this mode, no pressure variation is assumed along the channel (z-direction). However, gas species accumulation (transient regime) is taken into account using the following molar balance in the anode channel volume:

$$V_{ch} \frac{P_{tot}}{R T_{op}} \frac{\partial y_i}{\partial t} = Q_i^m - N_i A_m \quad (22)$$

where V_{ch} is the channel volume (m^3). In both flow-through and dead-end modes, the boundary conditions of the channel transport model are the fluxes exchanged between the channel and the GDLs as well as the channel inlet conditions (SR^{in} , RH^{in} , P_{tot}^{in} , y^{in}) which give Q_i^m and y_i^m .

2.5 Simulation conditions

The coupled equations described above are solved numerically by a finite difference method with implicit scheme and coded in C programming language. The model is run in the Matlab-Simulink environment to solve the algebraic loops. For all the results shown hereafter, in addition to the individual parameters analyzed in each paragraph, the reference operating conditions used are given in Table 1. Relevant parameters describing the modeled fuel cell are listed in Table 2.

Table 1. Reference operating conditions

Parameter	Symbol	Units	Value in H ₂ dead-end mode	Value in H ₂ flow-through mode
Anode inlet gas pressure	P_{an}^{in}	<i>kPa</i>	101.325	101.325
Cathode inlet gas pressure	P_{cat}^{in}	<i>kPa</i>	101.325	101.325
Anode inlet relative humidity	RH_{an}^{in}	-	0	0.5
Cathode inlet relative humidity	RH_{cat}^{in}	-	0.5	0.5
Hydrogen stoichiometric ratio	SR_{H_2}	-	1	2
Oxygen stoichiometric ratio	SR_{O_2}	-	2	2
Hydrogen inlet moalr fraction	$y_{H_2}^{in}$	-	1	1
Oxygen inlet moalr fraction	$y_{O_2}^{in}$	-	0.21	0.21
Cell operating temperature	T_{op}	<i>K</i>	333.15	333.15

Table 2. Model parameters

Parameter	Symbol	Units	Value
Membrane active area	A_m	<i>m</i> ²	78 10 ⁻⁴
Membrane thickness	L_m	<i>m</i>	37 10 ⁻⁶
GDL thickness	L_{GDL}	<i>m</i>	280 10 ⁻⁶
GDL porosity	ε	-	0.5
Anode channels cross section area	$A_{ch,an}$	<i>m</i> ²	1.4 10 ⁻⁶
Cathode channels cross section area	$A_{ch,cat}$	<i>m</i> ²	1.344 10 ⁻⁶
Anode channels length	$L_{ch,an}$	<i>m</i>	1.158
Molecular weight of dry membrane	EW	<i>kg.mol</i> ⁻¹ _{SO₃}	0.9
Density of dry membrane	ρ_m	<i>kg.m</i> ⁻³	2800
Membrane permeability	K	<i>m</i> ²	1.58 10 ⁻¹⁸
Water viscosity	μ	<i>kg.m</i> ⁻¹ . <i>s</i> ⁻¹	4.71 10 ⁻⁴
Mass transfer coefficient between GDL and gas channel in the anode	$h_{m,an}$	<i>m.s</i> ⁻¹	1.2
Mass transfer coefficient between GDL and gas channel in the cathode	$h_{m,cat}$	<i>m.s</i> ⁻¹	0.09

3. Results and discussion

3.1 Liquid water appearance and critical current

Since the most critical constraint on power cell operation comes from the presence of water, the conditions under which liquid water appears in the cell were investigated. This section presents these results and shows how to relate liquid water appearance to ideal operating conditions.

these studies, no results are analyzed in term of internal water cell management leading to accurate membrane hydration without excess water in the electrodes. The present model allows to analyze liquid water appearance in any location throughout the cell. Thus, the two next sections (sections 3.1.2 and 3.1.3) focus on finding a pertinent location allowing to interpret the appearance of liquid water in terms of an ideal operating point.

3.1.2 Onset of two-phase regime in the electrodes

As mentioned in section 3.1.1, water first appears at the catalyst layer close to the channel's outlet (point C in Figure 2). The present model therefore computes the threshold current density corresponding to the first appearance of liquid water at point C for different oxygen stoichiometric ratios SR_{O_2} and temperatures T_{op} (Figure 3). Water production is obviously directly related to the current density: the higher the current, the more water has to be removed from the cell. As long as the vapor pressure is below the saturation pressure, water is present in the gaseous phase only. On the other hand, when the saturation pressure is reached, water condenses in the cell and both phases are present. It therefore exists a threshold current which triggers the development of two-phase flows [13].

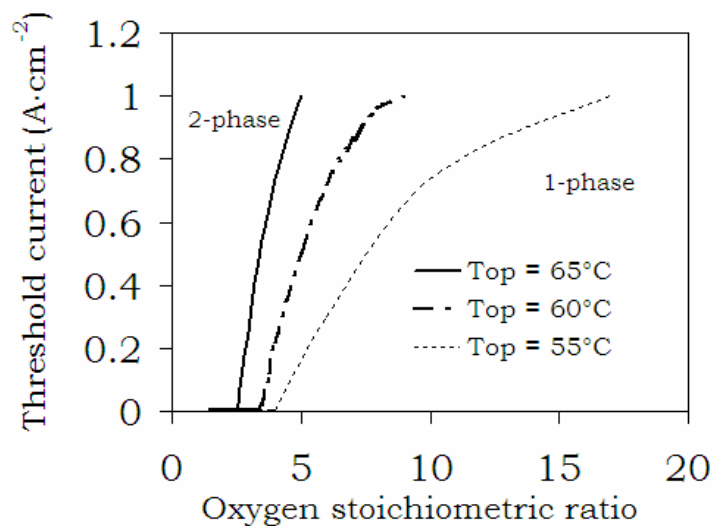


Figure 3. Threshold current for the first liquid droplet appearance in the cell

Figure 3 shows how the threshold current increases versus the oxygen stoichiometric ratio, for three operating cell temperatures (T_{op}). The results show a strong dependence of this threshold current on temperature because of the strong dependence of the saturation pressure on temperature (as described in equation (11)). Similar results were obtained in [13] and [11]. With the help of Figure 3, for a given current and temperature, the minimum stoichiometric ratio necessary to avoid liquid water in the whole cell can be known. For example, in order to keep the cell without liquid water at 60°C and for intermediate currents (around 0.5 A·cm⁻²), it is sufficient to hold the oxygen stoichiometric ratio at a minimum of 5. For high currents (around 1 A·cm⁻²), the stoichiometric ratio has to be increased up to 10 in order to avoid water condensation. This threshold stoichiometric ratio is also strongly temperature dependent: for 55°C, the ratio increases up to 17, whereas for 65°C, a ratio of 5 is enough (still at high currents).

This analysis leads to the conclusion that, in general cases where the oxygen stoichiometric ratio is between 2 and 3, liquid water will exist in the cell for intermediate and high currents. However, the presence of liquid water is not intrinsically damageable to the cell. Flooding, where the liquid water produces dramatic voltage degradation, appears only once there is a certain amount of liquid water in the cell, and not just as soon as the first droplet appears [12]. In addition, reasonable amounts of liquid water can have good effects on the cell voltage by decreasing the membrane resistance [15]. Therefore, the first appearance of water droplets at the catalyst layer close to the channel outlet (point C on Figure 2) does not correspond to a critical operating point. Hence, as it will be explained in the next section, it is desirable to analyze other locations in order to signal the threshold for liquid water appearance.

3.1.3 Critical operating current

Because the onset of the two-phase regime in the whole cell is not a critical aspect for the cell operation, it is useful to develop another approach where liquid water appearance could be analyzed in terms of ideal operating conditions.

As explained in earlier sections, accurate water content is required to decrease the membrane resistance, but excess water in the GDL is harmful for mass transport. The influence of the internal cell humidification on the cell performances can be examined through the current density progression along the channel (z -direction) as presented by Sun et al. [15]. For an under-humidified cell, the local current increases monotonously along the channel. Indeed, the membrane hydration level at the inlet A is low; this means a low local current density. Further along the channel towards B, as liquid water is produced, the membrane hydration increases progressively, yielding a higher local current density. On the other hand, for an over-hydrated cell, the local current decreases along the channel. Indeed, oxygen concentration decreases along the channel due to oxygen consumption and because the water content in the CL increases due to water production inherent to the cell's operation. This decrease of oxygen concentration results in a decrease of the current density. Moreover, there are also cases where the current increases in a first part of the channel, reaches a maximum, and then decreases further along the channel. In these cases, the two opposite effects of cell hydration (drying and flooding) are both locally present, but the cell is not strictly over-humidified or under-humidified. The maximum current density is found near the point in the z -direction where liquid water first appears in the CL. Indeed, at this point, the membrane is well humidified and there is no excess liquid water to prevent gas transport. In order to reach a good compromise between drying at the inlet and flooding near the outlet, it is therefore assumed that optimal internal humidification conditions are reached when liquid water appears at the cathode in the middle of the cell along the channel direction (point F in Figure 2). In accordance with the discussion above, the threshold current density involving liquid water appearance at point F (Figure 2) will be computed for different operating conditions. This threshold current density will be called the critical current density, and denoted by i_{cr} . For any operating conditions, if the operating current is lower than the critical current, there is no liquid water in the middle of the cell along the channel. This is interpreted in this work as an under-humidified cell and may lead to drying. On the other hand, if the operating current is higher than the critical current, liquid water is present in more than one half of the channel. This is interpreted in this work as an over-humidified cell and may lead to flooding. The critical current computed in this paper is therefore assumed to be the ideal current for the given operating conditions.

Further developments on that ideal humidification conditions assumption will be addressed in later papers. However, no matter which assumption is used, the trend of the next results, like the parameters influences, will remain unchanged. Hence, the results below are useful to analyze the role that each operating parameters can play in the cell internal humidification management.

3.2 Critical current analysis

In this section, the effects of the operating parameters (inlet humidities, stoichiometric ratio, temperature and pressures) on the critical current are presented. This allows to quantify the operating parameters effects on the internal cell hydration and to determine operating parameters resulting in the ideal cell internal humidification (accurate membrane hydration without liquid water excess).

3.2.1 Effect of the inlet relative humidities

It is expected that the inlet relative humidities influence the cell internal humidification, but their effects may be very different according to the hydrogen supply mode.

Hydrogen dead-end mode

Figure 4 shows the critical current density i_{cr} ($A \cdot cm^{-2}$) for different inlet relative humidities respectively at the cathode RH_{cat}^{in} and at the anode RH_{an}^{in} . The other operating parameters are summarized in tables 1 and 2 (in particular, the operating temperature is $60^\circ C$ and the oxygen stoichiometric ratio is 2).

Three different zones are observed in Figure 4. For low cathode relative humidities, the critical current is higher than $1 A \cdot cm^{-2}$ no matter what the anode inlet humidity is. The cell is therefore under-humidified (for currents lower than $1 A \cdot cm^{-2}$). On the contrary, for high cathode relative humidities, the critical current tends towards 0. The cell is therefore over-humidified (for currents higher than $0.005 A \cdot cm^{-2}$). A

third medium zone exists where the critical current varies from 0 to 1 A·cm⁻² depending on the inlet relative humidities. For any pair of relative humidities in this zone, the operating current has to be accurately chosen in order to reach the appropriate operating conditions. Inversely, for any operating current density, the inlet relative humidities can be accurately chosen in this third zone to reach the ideal conditions.

Anode inlet relative humidity	1	>1	1	0.78	0.52	0.26	0.04	0.005	0.005	<0.005	<0.005	<0.005
	0.9	>1	>1	0.82	0.54	0.3	0.04	0.005	0.005	<0.005	<0.005	<0.005
	0.8	>1	>1	0.88	0.58	0.34	0.04	0.005	0.005	<0.005	<0.005	<0.005
	0.7	>1	>1	0.92	0.64	0.38	0.06	0.02	0.01	0.005	0.005	<0.005
	0.6	>1	>1	0.98	0.7	0.4	0.1	0.02	0.005	0.005	0.005	<0.005
	0.5	>1	>1	1	0.72	0.44	0.14	0.02	0.005	0.005	0.005	<0.005
	0.4	>1	>1	>1	0.76	0.48	0.16	0.02	0.005	0.005	0.005	<0.005
	0.3	>1	>1	>1	0.8	0.52	0.18	0.04	0.005	0.005	0.005	<0.005
	0.2	>1	>1	>1	0.84	0.54	0.2	0.04	0.005	0.005	0.005	<0.005
	0.1	>1	>1	>1	0.88	0.58	0.24	0.04	0.005	0.005	0.005	<0.005
	0	>1	>1	>1	0.94	0.6	0.3	0.04	0.005	0.005	0.005	<0.005
	0	0.1	0.2	0.3	0.4	0.5	0.6	0.7	0.8	0.9	1	
	Cathode inlet relative humidity											

Figure 4. Critical current density (A·cm⁻²) for different inlet relative humidities (dead-end mode)

According to the results of Figure 4, the cathode relative humidity has a much greater influence on the critical current than the anode one (in steady state). This is because of the cathode humidity's important effect on the water pressure profile, as indicated by the relatively large vertical separation of the two tracks in the membrane, the GDLs and the channels (Figure 5). On the contrary, the anode humidity has a low influence on the critical current because it has a very little impact on water distribution in the cell (Figure 6).

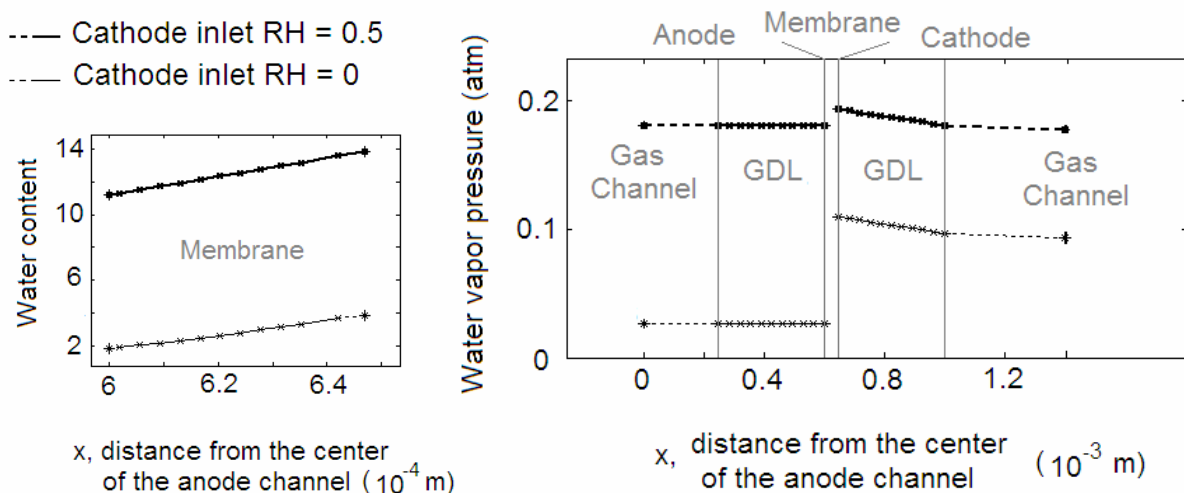


Figure 5. Influence of the inlet cathode relative humidity on the water content in the membrane and on water vapor profile in the electrodes at the center of the cell (anode inlet relative humidity is 0 and $i = 0.3$ A·cm⁻²)

Comparing these two cases (Figure 5 and Figure 6) shows that the cathode inlet RH is a very significant factor in influencing the water vapor pressure and the water content (the difference between the two water content curves in Figure 5 is of the order of 400%), whereas the anode inlet RH is not significant (the difference in Figure 6 is of the order of 5%). This is due to the fact that, in dead end mode, the water accumulates in steady state at the anode side up to a certain level which creates a diffusive flux allowing to balance the electro-osmotic flux. Another reason is that the water flux created in the membrane by the inlet water content is non-significant versus the electro-osmotic flux and the production flux (for common operating conditions). No anode humidification is therefore required in a dead-end mode in steady state.

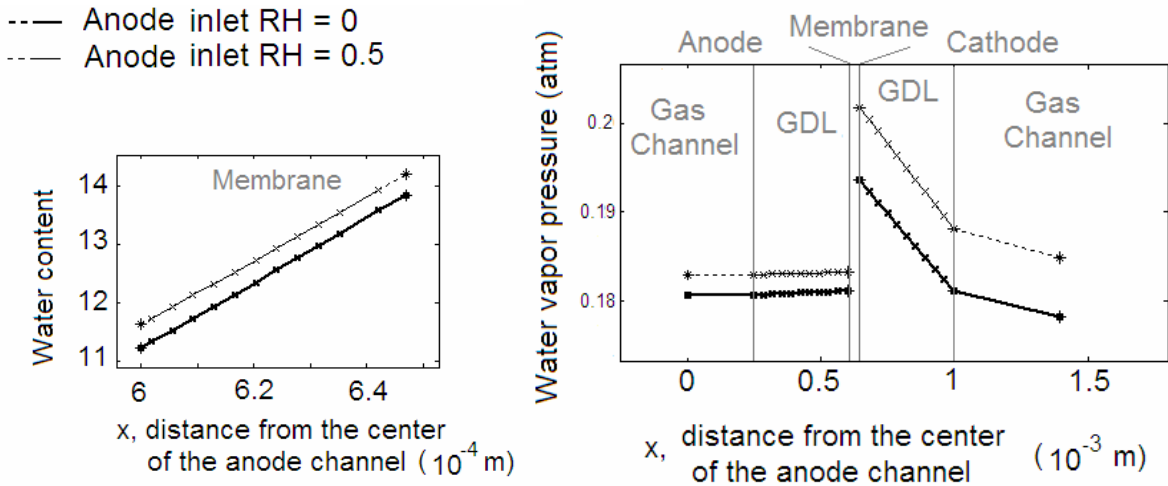


Figure 6. Influence of inlet anode relative humidity on water vapor profile in the electrodes and on the water content in the membrane (cathode inlet relative humidity is 0.5 and $i = 0.3 \text{ A}\cdot\text{cm}^{-2}$)

Hydrogen flow-through mode

Figure 7 presents the critical current density i_{cr} for different inlet cathode and anode relative humidities RH_{cat}^{in} and RH_{an}^{in} when hydrogen is supplied in a flow-through mode.

Anode inlet relative humidity	1	>1	0.86	0.66	0.46	0.22	0.04	0.005	<0.005	<0.005	<0.005	<0.005
	0.9	>1	0.96	0.76	0.56	0.32	0.08	0.005	0.005	<0.005	<0.005	<0.005
	0.8	>1	>1	0.86	0.66	0.4	0.16	0.02	0.005	0.01	0.005	<0.005
	0.7	>1	>1	0.98	0.76	0.52	0.26	0.04	0.01	0.005	0.005	<0.005
	0.6	>1	>1	>1	0.88	0.64	0.36	0.1	0.005	0.005	0.005	0.005
	0.5	>1	>1	>1	0.98	0.72	0.48	0.18	0.02	0.005	0.005	0.005
	0.4	>1	>1	>1	>1	0.86	0.56	0.3	0.04	0.005	0.005	0.005
	0.3	>1	>1	>1	>1	0.96	0.72	0.4	0.08	0.005	0.005	0.005
	0.2	>1	>1	>1	>1	>1	0.82	0.54	0.22	0.02	0.005	0.005
	0.1	>1	>1	>1	>1	>1	0.94	0.66	0.34	0.04	0.005	0.005
0	>1	>1	>1	>1	>1	>1	0.78	0.48	0.1	0.005	0.005	
		0	0.1	0.2	0.3	0.4	0.5	0.6	0.7	0.8	0.9	1
		Cathode inlet relative humidity										

Figure 7. Critical current density ($\text{A}\cdot\text{cm}^{-2}$) for different inlet relative humidity (flow-through mode)

It is seen that the dependence of the critical current density on the humidities is qualitatively similar to the dead-end mode. Nevertheless, some differences exist. The anode relative humidity has more influence in flow-through mode than in dead-end mode. However, this influence is still less than the influence of the cathode relative humidity. Except for high anode humidifications, the critical current density at a given value of cathode humidity is higher in flow-through mode than in dead-end mode. Flow-through mode thus tends to decrease the internal cell humidification since the gas flow removes water from the cell. For high anode relative humidifications, the critical current is lower, implying a higher cell internal humidification due to the fact that more water is added into the cell.

3.2.2 Effect of the stoichiometric ratios

In both hydrogen supply modes, the stoichiometric ratios influence water removal from the electrodes, and accordingly, the critical current. In this section, dead-end and flow-through configurations are studied separately because the hydrogen stoichiometric ratio can vary only in the flow-through configuration.

Hydrogen dead-end mode

Figure 8 shows the influence of the oxygen stoichiometric ratio on the critical current density for different cathode relative humidities (see Table 1 for the others operating parameters).

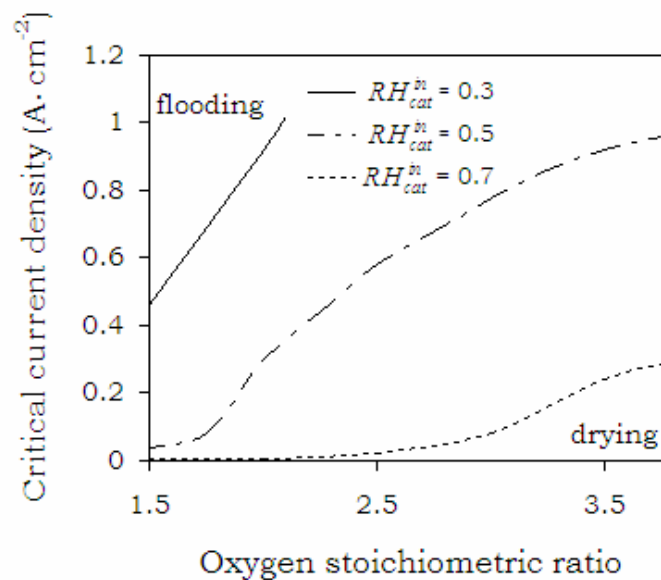


Figure 8. Influence of the oxygen stoichiometric ratio on the critical current density

This figure shows that, for a 50% cathode relative humidity, the oxygen stoichiometric ratio can be chosen to reach any critical current density in the range of 0 to 1 A·cm⁻². However this is not the case for some other cathode relative humidities. For a low cathode inlet humidification (30%), the critical current density is always above 0.4 A·cm⁻², no matter what the stoichiometric ratio is. This implies that for low currents, the cell will always be under-humidified. On the other hand, for a high cathode inlet humidification (70%), the critical current density is always below 0.3 A·cm⁻², no matter what the stoichiometric ratio is, and the cell will thus be over-humidified for high currents. Clearly, optimal humidification conditions cannot be reached merely by changing the oxygen stoichiometric ratio.

Hydrogen flow-through mode

Figure 9 presents the influence of the hydrogen and oxygen stoichiometric ratios on the critical current density in flow-through mode hydrogen supply. The influence of the oxygen stoichiometric ratio in dead-end mode of hydrogen supply is also reported for comparison (see Table 1 for the others operating parameters).

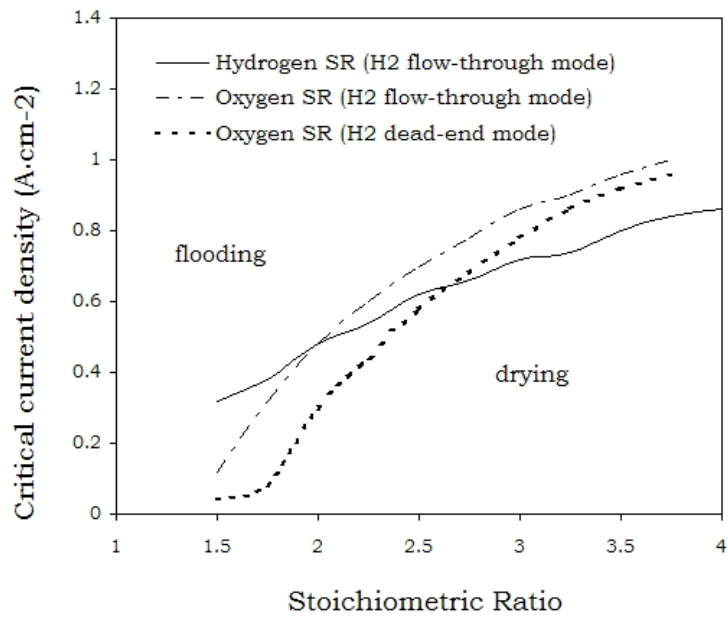


Figure 9. Influences of the stoichiometric ratios

First, it can be seen that the oxygen stoichiometric ratio has almost the same influence in dead-end mode as in flow-through mode. Indeed, increasing the oxygen stoichiometric ratio results in better water removal from the channels. This effect is the same no matter how the hydrogen is supplied.

Secondly, the hydrogen stoichiometric ratio has less influence on the critical current than the oxygen ratio. Indeed, there is no inert gas present in the supplied hydrogen (compared to oxygen), and the mechanisms involved in water distribution in the cell are not symmetrical (water production at the cathode and electro-osmotic drag toward the cathode). Accordingly, tuning the hydrogen stoichiometric ratio can be less efficient than tuning the oxygen one in order to adjust cell humidification conditions.

3.2.3 Effect of the temperature

The cell internal humidification is thermo-dependent as a consequence of the water saturation pressure thermo-dependency. The critical current will therefore depend on the temperature. The influence of the temperature on the critical current is presented in Figure 10 for different cathode relative humidities (the anode relative humidity is 0 and hydrogen is supplied in a dead end mode - see Table 1 for the others operating parameters).

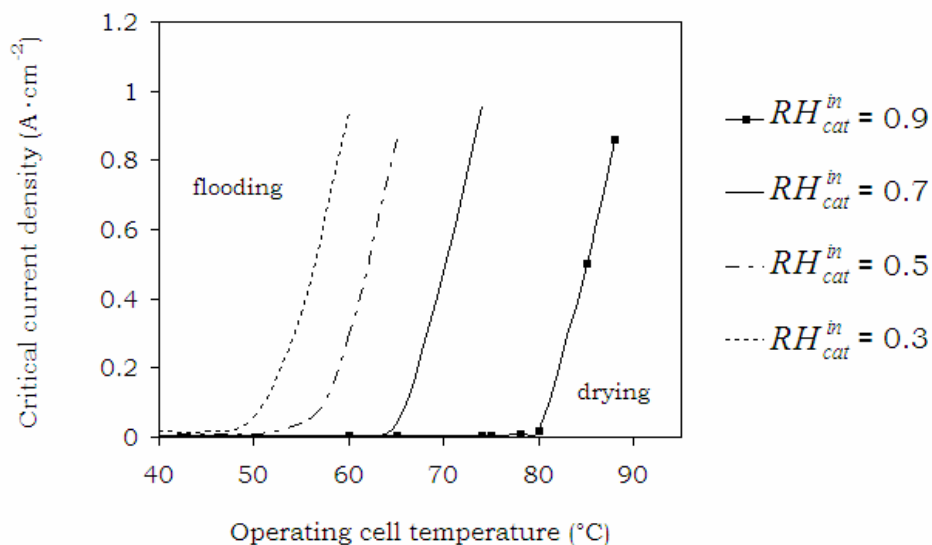


Figure 10. Temperature effect on the critical current (dead end mode of hydrogen supply)

The critical current density is extremely dependent on temperature because of the exponential dependency of the saturation pressure, as shown in (11). The result is that the critical current varies from 0 to 1 A·cm⁻² within a narrow temperature range of only 10°C, the onset of the change depending on the value of the cathode relative humidity (the higher that value, the higher the onset temperature). This implies that a small change in temperature for the same operating current can lead to a drastic change in the cell humidification conditions, changing from flooding to drying or inversely. Similar results are obtained in a hydrogen flow-through mode. Hence, temperature control can be very efficient to solve cell degradations due to water faults. This highlights the importance of heat management in fuel cells.

3.2.4 Effect of the total pressure

Pressure is another operating parameter which could influence the critical current. Simulations were conducted for various cathode and anode inlet total pressures (“total pressure” here means the sum of all the partial pressures at any electrode). Pressures are considered only up to 200 kPa because many fuel cells operate around atmospheric pressure in order to reduce compressor energy consumption.

As shown in Figure 11, the anode and cathode total pressures (kept equal) also have an important influence on the critical current. (Note that, once again, all the other parameters remain constant - see Table 1 for the values - and particularly, the oxygen stoichiometric ratio is set at 2). Still, the influence of the pressure is roughly the same in both hydrogen supply modes.

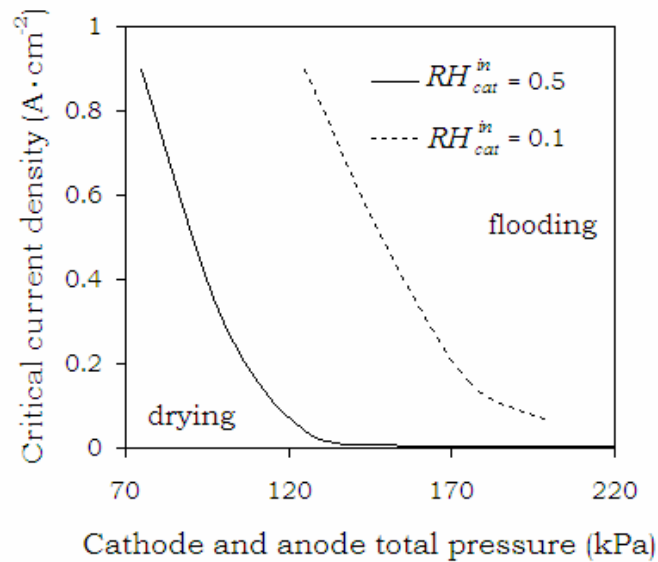


Figure 11. Total pressure effect on the critical current (dead end mode of hydrogen supply)

The decrease of the critical current versus the total pressure is explained via the gas velocity in the channel. Indeed, let's consider two operating conditions where only the total pressure is different. First, a change in the total pressure does not lead to a change in the inlet vapor partial pressure since the latter depends only on the relative humidity and on the temperature as given by equation (23) (the saturation pressure depends on temperature only and not on total pressure):

$$P_2^{in} = RH_{in} \times P_{sat}(T_{op}) \quad (23)$$

It does not lead either to a change in the water production $N_{H_2O}^{prod}$ based on (24):

$$N_{H_2O}^{prod} = \frac{i}{2F} \quad (24)$$

Hence, the input water content is the same in both cases. On the other hand, the water removal is changed. Indeed, the cathode flow rate is given by equation (25).

$$Q_{tot} = \frac{P_{tot}}{RT_{op}} v_{tot} A_{ch} \quad (25)$$

So, the cathode velocity is:

$$v_{tot} = \frac{Q_{tot}}{P_{tot}} \frac{RT_{op}}{A_{ch}} \quad (26)$$

A high total pressure therefore produces a low velocity (the total molar flow is approximately the same since the stoichiometric ratio is constant). Now, the water removed from the cell by air is given by:

$$Q_{H_2O} = \frac{P_{H_2O}}{RT_{op}} v_{tot} A_{ch} \quad (27)$$

Lower velocity yields a lower water removal rate, and so the water vapour pressure in the electrode is higher. Finally, this higher water vapour pressure results in a lower critical current density according to its definition.

3.3 Humidification strategies

To obtain good membrane humidification, it is common to think that hydrogen has to be humidified and supplied in flow-through mode [28]. The results in the present study suggest that a good membrane humidification can also be obtained with dead-end mode. The present section compares these different strategies.

Figure 12 shows the water content profile in the membrane (x-direction) for a $0.3 \text{ A}\cdot\text{cm}^{-2}$ current density and for different humidification conditions (the operating parameters are given in the previous Tables 1 and 2). The profile is the one at the coordinate z corresponding to the center of the cell along the channel direction.

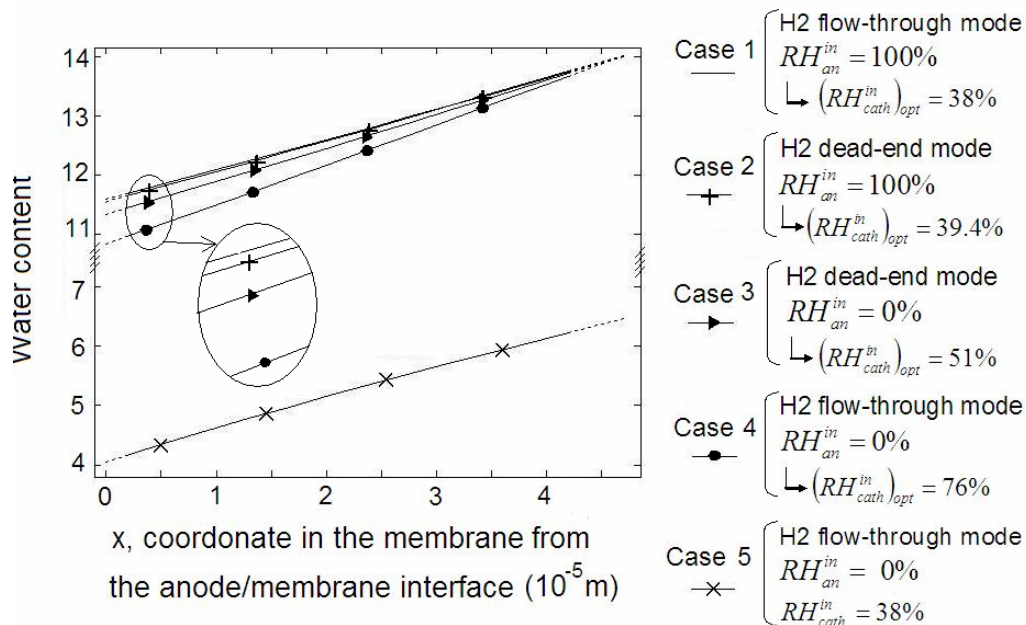


Figure 12. Water content profile in the membrane for different humidification conditions

For cases 1 to 4, the operating current corresponds to the critical current, i.e. the ideal current leading to water balance in the cell related to the operating conditions. Thus, the four cases are ideal cases for four different humidification strategies: flow-through mode with fully humidified hydrogen (case 1), dead-end mode with fully humidified hydrogen (case 2), dead-end mode without anode humidification (case 3), and flow-through mode without anode humidification (case 4).

The cases with a 100% anode inlet humidification ratio (cases 1 and 2) lead to the best membrane humidification. However, their profiles are only a few per cent better than those for 0% anode humidification (cases 3 and 4). Hence all four cases also give reasonably similar ohmic losses, even at high current densities (within 5% at $1 \text{ A}\cdot\text{cm}^{-2}$).

Conventional wisdom has it that anode inlet humidification is required to prevent membrane drying near the anode, particularly at high current densities where an important electro-osmotic drag exists [28]. This is clear by comparing cases 1 and 5 (at the same cathode inlet humidification of 38%). On the other hand, the same performances can be achieved without anode humidification simply by changing the cathode humidification, as shown by comparison of cases 1 and 4 (with 76% cathode humidification).

Since the performance for each humidification strategy (flow-through or dead-end with hydrogen saturated or not) is almost the same for the ideal operating conditions, it can be concluded that humidifying the anode inlet is not significantly important. Hence, instead of using a hydrogen flow-through mode with a recirculation and humidification system at the anode, a simpler hydrogen dead-end mode with no anode humidification can be used. Only an adjustment of the cathode humidification is necessary in this case. This concluding remark is of a great interest for fuel cell design. According to this observation, the fuel cell system can largely be reduced and simplified for the same performances. Note that it is the strategy used by Ballard with the NEXA fuel cell [29]. However, purges have to be done and optimized to regularly remove water and inert gases.

4. Conclusions and perspectives

A dynamic pseudo 2D model of a polymer electrolyte membrane fuel cell is presented in this work. This model describes multi-component gas transport in the gas diffusion layers and in the bipolar plate channels. It also describes water transport in the membrane. This model is used to analyze the role that each operating parameters can play in the cell internal humidification management and consequently, the cell performances.

For that purpose, a discussion is opened about the effect of liquid water appearance at different locations in the cell on the voltage. According to this analysis, it is proposed that the ideal internal humidification conditions are reached when liquid water appears in the middle of the cell along the channel. This appears to be a good compromise between flooding and drying. The critical current density which yields this ideal internal humidification is then computed for various operating conditions. The influence of the various operating parameters on this critical current, such as gas inlet relative humidities, temperature, stoichiometric ratios or pressures, is analyzed. In the analysis, dead-end and flow-through modes of hydrogen supply are also compared.

Operating cell temperature has a strong influence on the critical current and can dramatically influence the internal humidification of the cell. Hence, the temperature is a key parameter to control when considering the cell internal humidification. It is shown that the cathode total pressure also has a significant influence. Moreover, although the oxygen stoichiometric ratio has an effect on cell humidification, this influence is limited and cannot be used alone to adjust the cell humidification.

In contrast to the cathode inlet humidification, the anode inlet humidification has almost no influence in a dead-end hydrogen configuration; its influence in a flow-through mode is not significant either. In addition, it is found that, instead of using a hydrogen flow-through mode with a recirculation and humidification system at the anode, a simpler hydrogen dead-end mode with no anode humidification can be used to obtain almost the same membrane humidification. An adjustment of the cathode humidification is necessary in this case. Indeed, the anode is prevented from drying at high current density due to the water diffusion from the cathode toward the anode.

All these results are of great interest to the improvement of water management in PEMFC. They lead to a better understanding of how to use the operating parameters to control the cell internal humidification. These results are also useful to develop control humidification strategies by simulating different humidification approaches. In a future part of this work, liquid water transport will be modeled for a more precise determination of the optimum operating conditions. This will allow to take into account voltage drops due to flooding. Furthermore, a transient analysis of the internal humidification will be conducted. Finally, this simple control-oriented model will be used by a real time control algorithm to command the fuel cell operating parameters in order to improve the overall system efficiency.

Acknowledgements

This work was jointly supported by LTE-Hydro-Quebec and Natural Sciences and Engineering Research Council of Canada. The authors gratefully acknowledge the advices of Michel Dostie, Michael Fournier and Alain Poulin from the LTE Hydro-Québec.

References

- [1] Barbir F. PEM fuel cells: theory and practice. Elsevier Academic Press, 2005.
- [2] Ramousse J., Adzakpa K.P., Dube Y., Agbossou K., Fournier M., Poulin A., Dostie M. Local voltage degradations (drying and flooding) analysis through 3D stack thermal modeling, Accepted for publication in J. Fuel Cell Science and Technology 2009.
- [3] Bernardi D.M., Verbrugge M.W. A mathematical model of the solid-polymer-electrolyte fuel cell. J. Electrochem. Soc., 1992, 139, 2477-2491.
- [4] Springer T.E., Zawodzinski T.A., Gottesfeld S. Polymer electrolyte fuel cell model. J. Electrochem. Soc. 1991, 138, 2334-2342.
- [5] Fuller T.F., Newman J. Water and thermal management in solid-polymer-electrolyte fuel cells. J. Electrochem. Soc. 1993, 140, 1218-1225.
- [6] Nguyen T.V., White R.E. A water and heat management model for proton-exchange-membrane fuel cells. J. Electrochem. Soc. 1993, 140, 2178-2186.
- [7] Adzakpa K.P., Ramousse J., Dubé Y., Akremi H., Agbossou K., Dostie M., Poulin A. Fournier M. Transient air cooling thermal modeling of a PEM fuel cell. J. Power Sources 2008, 179, 164-176.
- [8] Natarajan D., Van Nguyen T. Three-dimensional effects of liquid water flooding in the cathode of a PEM fuel cell. J. Power Sources 2003, 115, 66-80.
- [9] Sun H., Liu H., Guo L.-J. PEM fuel cell performance and its two-phase mass transport. J. Power Sources 2005, 143, 125-135.
- [10] Dunbar Z., Masel R.I. Quantitative MRI study of water distribution during operation of a PEM fuel cell using Teflon(R) flow fields. J. Power Sources 2007, 171, 678-687.
- [11] Tuber K., Poczka D., Hebling C. Visualization of water buildup in the cathode of a transparent PEM fuel cell. J. Power Sources 2003, 124, 403-414.
- [12] Owejan J.P., Trabold T.A., Gagliardo J.J., Jacobson D.L., Carter R.N., Hussey D.S., Arif M. Voltage instability in a simulated fuel cell stack correlated to cathode water accumulation. J. Power Sources 2007, 171, 626-633.
- [13] Wang Z.H., Wang C.Y., Chen K.S. Two-phase flow and transport in the air cathode of proton exchange membrane fuel cells. J. Power Sources 2001, 94, 40-50.
- [14] Pasaogullari U., Wang C.-Y. Liquid water transport in gas diffusion layer of polymer electrolyte fuel cells. J. Electrochem. Soc. 2004, 151, A399-A406.
- [15] Sun H., Zhang G., Guo L.-J., Dehua S., Liu H., Effects of humidification temperatures on local current characteristics in a PEM fuel cell. J. Power Sources 2007, 168, 400-407.
- [16] Lee C.-I., Chu H.-S. Effects of cathode humidification on the gas-liquid interface location in a PEM fuel cell. J. Power Sources 2006, 161, 949-956.
- [17] Lee C.-I., Chu H.-S. Effects of temperature on the location of the gas-liquid interface in a PEM fuel cell. J. Power Sources 2007, 171, 718-727.
- [18] Williams M.V., Kunz H.R., Fenton J.M., Operation of Nafion®-based PEM fuel cells with no external humidification: influence of operating conditions and gas diffusion layers. J. Power Sources 2004, 135, 122-134.
- [19] Fournier M., Agbossou K., Poulin A., Dubé Y., Simard G. Dynamic model of a PEMFC stack suitable for component level modeling of a fuel cell based generator. Proceedings of the 16th World Hydrogen Energy Conference. Lyon, France, 2006.
- [20] Song D., Wang Q., Liu Z.-S., Huang C. Transient analysis for the cathode gas diffusion layer of PEM fuel cells. J. Power Sources 2006, 159, 928-942.
- [21] Weber A.Z., Newman J. Modeling transport in polymer-electrolyte fuel cells. Chem. Rev. 2004, 104, 4679-4726.
- [22] B.M. Eaton. One dimensional transient model of heat, mass, and charge transfer in a proton exchange membrane. M. of Sc. Thesis, Virginia Polytechnic and State University, 2001.
- [23] Nam J.H., Kaviany M. Effective diffusivity and water-saturation distribution in single- and two-layer PEMFC diffusion medium. Int. J. Heat Mass Transfer 2003, 46, 4595-4611.
- [24] Bird R.B., Stewart W.E., Lightfoot E.N. Transport phenomena. John Wiley & sons, 1960.

- [25] Chang M.-H., Chen F., Teng H.-S. Effects of two-phase transport in the cathode gas diffusion layer on the performance of a PEMFC. *J. Power Sources* 2006, 160, 268-276.
- [26] Hassanaly N., Agbossou K., Dube Y., Adzakpa K.P. Air Supply state model for a proton exchange membrane fuel cell control, *Proceedings of the Canadian Conference on Electrical and Computer Engineering*. Vancouver, Canada, 2007. p. 1511-1514.
- [27] Karnik A.Y., Stefanopoulou A.G., Sun J. Water equilibria and management using a two-volume model of a polymer electrolyte fuel cell. *J. Power Sources* 2007, 164, 590-605.
- [28] You L., Liu H. A two-phase flow and transport model for the cathode of PEM fuel cells. *Int. J. Heat Mass Transfer* 2002, 45, 2277-2287.

Florent Breque received his bachelor degree in Mechanical and Aeronautical Engineering at ENSMA (Ecole Nationale Supérieure de Mécanique et d'Aérotechnique), Poitiers, France, in early 2005. In the same time, he specialized at McGill University in Montréal (Canada) in fluid mechanics, energetics and heat transfer.

He was a research engineer at European Aeronautic Defence and Space Company (EADS). Then he joined the Hydrogen Research Institute IRH (Institut de Recherche sur l'Hydrogène), Trois-Rivières, Canada, in 2006 as a Master student. His research includes numerical modelling and control aspects of polymer electrolyte membrane fuel cells. He mainly focuses on mass transfer in order to improve water management in a fuel cell. His work is supported by Hydro-Québec, Natural Resources Canada and the Natural Sciences and Engineering Research Council of Canada.

E-mail address: Florent.Breque@mdacorporation.com

Julien Ramousse received the B.Sc. and M.Sc. degrees in energetics and mechanical engineering from the Ecole Nationale Supérieure d'Électricité et de Mécanique (ENSEM), Nancy, France, in 2002, and the Ph.D. degree from the Institut National Polytechnique de Lorraine (INPL), Nancy, France, in 2005. He worked in the Hydrogen Research Institute, Université du Québec à Trois-Rivières, Trois-Rivières, QC, Canada, from September 2006 to 2008 as a Postdoctoral Researcher. Since September 2008, he is an Assistant Professor at the engineering school Polytech'Annecy-Chambéry, Université de Savoie, Chambéry, France.

His research, now done at the Laboratoire Optimisation de la Conception et Ingénierie de l'Environnement (LOCIE) concerns transfer intensification in energy conversion devices. His research fields include mainly mass transfer in order to improve water management in fuel cells, numerical modeling and control aspects of PEMFC systems, and recently heat transfer in thermoelectric heat pumps. He is the co-author of almost 10 publications with more than 30 conference presentations.

Dr. Ramousse is a member of the Editorial Advisory Board of the International Journal of Energy and Environment (IJEE).

E-mail address: julien.ramousse@univ-savoie.fr

Yves Dube received his B.S. (1977) in physical engineering, M.S. (1979) in mechanical engineering and Ph.D. (1985) degree in Simulation and Control from the Université Laval in Canada. He is now Professor in the Mechanical Engineering Department of UQTR. His present research activities are in the area of renewable energy, hydrogen combustion engine development and control of mechanical systems. He is the author of more than 30 publications and has 1 patent. He is a Professional Engineer and member of the Ordre des Ingénieurs du Québec since 1977.

E-mail address: Yves.Dube@uqtr.ca

Kodjo Agbossou (M'1998, SM'2001) received his B.S. (1987), M.S. (1989) and Ph.D. (1992) degrees in Electronic Measurements from the Université de Nancy I, France. He was a post-doctoral researcher (1993-1994) at the Electrical Engineering Department of the Université du Québec à Trois-Rivières (UQTR), and was Lecturer (1997-1998) at the same department. Also he was Project Manager and Research Professional (1994-1998) in the Ultrasonic and Sensor Laboratory. Since 1998, he is Full Professor in the Electrical and Computer Engineering Department of UQTR. He was the Director of Graduate Studies in Electrical Engineering.

He is now a head of the department and his present research activities are in the area of renewable energy, integration of hydrogen production, storage and electrical energy generation system, control and measurements. He is the author of more than 70 publications and has 3 patents.

Pr. Agbossou is also a PES-IEEE member and former Chair of IEEE Section Saint Maurice, QC, Canada. He is a Professional Engineer and joined the Ordre des Ingénieurs du Québec in 1998.

E-mail address: Kodjo.Agbossou@uqtr.ca

Pelope Adzakpa received the B.Sc. and M.Sc. degrees in mathematics from the University of Lome, Lome, Togo, in 1998 and 1999, respectively, and the M.Sc. and Ph.D. degrees in industrial engineering from the University of Technology, Troyes, France, in 2001 and 2004, respectively. From 2000 to 2004, he was a Lecturer and a Research Assistant in the Industrial Systems Engineering Department, University of Technology, Troyes. From 2006 to 2007 he was a Postdoctoral Researcher at the Hydrogen Research Institute, Université du Québec à Trois-Rivières, Trois-Rivières, QC, Canada. He is currently a Comptia RFID+ Certified Professional in RFID software solutions. He is the author or coauthor of several publications. His research interests include industrial systems control, dependability and optimization, renewable-energy-system modeling, control, and diagnosis and RFID based ERP solutions.

E-mail address: pelope.adzakpa@axeti.com

